Seasonal and storm event-based dynamics of dissolved organic carbon (DOC) concentration in a Mediterranean headwater catchment

Alfonso Senatore[1], Giuseppina A. Corrente[2], Eugenio L. Argento[1], Jessica Castagna[1], Massimo Micieli[3,1], Giuseppe Mendicino[1], Amerigo Beneduci[2], Gianluca Botter[3]

[1] Department of Environmental Engineering, University of Calabria, Rende, Cosenza, Italy.

[2] Department of Chemistry and Chemical Technologies, University of Calabria, Rende, Cosenza, Italy.

[3] Department of Civil, Environmental and Architectural Engineering, University of Padua, Padua, Italy.

Corresponding author: Alfonso Senatore (alfonso.senatore@unical.it)

Key Points:

- More than two-year continuous high-frequency DOC monitoring in two nested sections with different topographic and land cover features
- Increasing background concentrations during dry summer, but top 10th percentile of discharge associated with up to 79% of total DOC yield
- Different DOC export processes in the two sections, with hysteretic behaviours non-linearly correlated with the antecedent precipitation

Keywords

Multi-parameter sondes, fDOM, DOC export, DOC hydrological control, hysteresis indices, generalized additive models GAM

Abstract

This study investigates the spatial and temporal dynamics of DOC concentration in a Mediterranean headwater catchment (Turbolo River catchment, southern Italy) equipped with two multi-parameter sondes providing more than two-year (May 2019 to November 2021) continuous high-frequency measurements of several DOC-related parameters. The sondes were installed in two nested sections, a quasi-pristine upstream sub-catchment and a downstream outlet with some anthropogenic disturbances on water quality. DOC estimates were achieved by correcting the fluorescent dissolved organic matter - fDOM - values through an original procedure not requiring extensive laboratory measurements. Then, DOC dynamics at the seasonal and storm event scales were analyzed. At the seasonal scale, results confirmed the climate control on DOC production, with increasing background concentrations in hot and dry summer months. The hydrological regulation proved crucial for DOC mobilization and export, with the top 10^{th} percentile of discharge associated with up to 79% of the total DOC yield. The analysis at the storm scale using flushing and hysteresis indices highlighted substantial differences between the two catchments. In the steeper upstream catchment, the limited capability of preserving hydraulic connection in time with DOC sources determined the prevalence of transport as the limiting factor to DOC export. Downstream, transport- and source-limited processes were observed almost equally. The correlation between the hysteretic behaviour and antecedent precipitation was not linear since the process reverted to transport-limited for high accumulated rainfall values. The study demonstrated the importance of high-resolution measurements to explain DOC dynamics at multiple time scales using a quantitative approach.

1 Introduction

Inland waters receive approximately 70% of the global annual terrestrial net ecosystem production (ca. 5.1 Pg of terrestrial carbon (C) per year; Soares et al., 2019). However, approximately only 1 Pg C is exported from the land to the ocean each year. 65% of exported C is dissolved, with 40% of it being organic (Chaplot and Mutema, 2021). The complex behaviour of dissolved organic carbon (DOC) within inland waters, which can be seen as “active pipelines” contributing to negative net ecosystem production (Cole et al., 2007), needs to be deeply investigated to improve the understanding of the global carbon cycle.

Hydrological factors are known to contribute to regulating the DOC balance at the reach scale (Bertuzzo et al., 2017; Parr et al., 2019). Interannual, intra-annual (seasonal) and event-based hydrological variability, particularly in headwater streams (Butman and Raymond, 2011; Rovelli et al., 2018), affects stream-hillslope organic matter exchanges and river network connectivity, leading to significant space and time variations in sources and processes regulating DOC dynamics. The impact of this interaction reflects on broader spatial scales so that, recently, regional approaches have been undertaken to evaluate the relationship between streamflow and DOC export regimes (Morison et al., 2022) or combine streamflow and DOC observations to validate catchment classification (Giesbrecht et al., 2022).

At different timescales, different processes emerge. At the seasonal scale, Viza et al. (2022) found that the intermittent flow regime of a Mediterranean river basin contributes to reducing organic matter decomposition rates. More generally, the effects of droughts on DOC

transport have being extensively investigated (e.g., Mehring et al., 2013; Humbert et al., 2015; Ahmadi et al., 2019; Wu et al., 2022). Available studies have highlighted the inhibition of DOC release during low flow conditions owing to reduced network connectivity but higher DOC concentrations after droughts.

Several studies reported DOC concentration increase in the last decades (e.g., Roulet and Moore, 2006; Monteith et al., 2007; Wu et al., 2022). This trend is connected to rising temperatures that favour the DOC release (Freeman et al., 2001; Bengtson and Bengtsson, 2007; Zhong et al., 2020; Chen et al., 2021), an instance which establishes positive feedback with climate change (since DOC is eventually converted into CO_2, a major greenhouse gas). Other causes, also linked to global warming, can concur to the observed increase of DOC export through the hydrological response, such as changes in land management, pH and sulfate, atmospheric CO_2 increase, acidic deposition decrease and runoff changes (Worral and Burt, 2007).

At short timescales of a few days or hours, storm events dominate DOC mobilization and transport (Parr et al., 2019). Precipitation activates direct wet deposition and indirect dry deposition deriving from vegetation canopy and stem (Song et al., 2021) and soil erosion (Chaplot and Mutema, 2021). This contribution to total DOC export is further emphasized if the wet event occurs at the end of prolonged dry periods (Blaurock et al., 2021). Fazekas et al. (2020) highlighted that anomalous events lasting overall less than 20 days in a year could define the annual behaviour of the relationships between streamflow and organic matter concentration.

For a specific basin, the concentration-discharge (C-Q) relationship is a signature of the interactions between biogeochemical and hydrological processes, which in their turn depend on climatic, geological and topographical features. C-Q relationships can reveal much of the DOC mobilization dynamics at different timescales (Chorover et al., 2017, Rose et al., 2017). At the seasonal or annual scale, null to low concentration variability in response to discharge fluctuations is called chemostasis (Godsey et al., 2009; Basu et al., 2010), indicating a homogeneous spatial distribution of DOC in the analyzed catchment. On the contrary, chemodynamic behaviour identifies stronger dependence of solute concentration on streamflow (Musolff et al., 2015; Fazekas et al., 2020). This behaviour is characterized by decreasing concentration with discharge if the DOC source is limited or, on the opposite, by increasing concentration with discharge if the limiting factor is the transport capacity. At the event scale, the hysteretic loop's shape and direction help identify the main transport mechanisms. E.g., if the DOC source is close and well-connected to the stream, clockwise hysteretic loops can be identified. On the contrary, counterclockwise loops prevail if it is far and connected by pathways with slow transport velocities.

The response of DOC dynamics is strictly connected to spatial features of heterogeneous ecosystems. Several studies showed that not only land cover type and land use (Aitkenhead-Peterson et al., 2007; Vaughan et al., 2017; Fovet et al., 2018; Seybold et al., 2019) but also local topography and geomorphic features (Weiler and McDonnell, 2006) significantly affect DOC mobilization and transport, influencing the hillslope-channel hydraulic connectivity (Botter et al., 2021). Therefore, the response in time of DOC dynamics in specific sections of a catchment is modulated by local properties of the upstream areas. Within the same catchment, significant differences can arise, which cannot be fully captured by a single downstream monitoring section that integrates heterogeneous upstream biogeochemical signals. It is a typical problem of scale (Lowe et al., 2006; McGuire et al., 2014), which also affects streamwater chemistry and needs to

be addressed with innovative theoretical concepts and technical approaches, including intensive spatially distributed monitoring campaigns in nested sections of the same catchment (McGuire et al., 2014; Blaurock et al., 2021).

DOC dynamics monitoring across different spatial and temporal scales is possible thanks to the advancements in optical aquatic sensors technology. Through in-situ continuous high-frequency measurements, such sensors catch rapidly changing concentrations during storm events and trends over more extended (seasonal to interannual) periods (Pellerin et al., 2014), supporting the development of accurate dynamic models (e.g., Jones et al., 2014) and, in general, providing great potential for a better understanding of aquatic ecosystems functioning (Snyder et al., 2018). Indeed, optical aquatic sensors do not measure DOC directly but rather the fluorescent dissolved organic matter (fDOM), the fraction of DOM that fluoresces. fDOM data can be corrected by accounting for some physical properties of the water (e.g., Watras et al., 2011; Downing et al., 2012; Snyder et al., 2018) and related to DOC using laboratory measurements needed to calibrate the transfer function. Many studies exploit optical sensor properties integrated into multi-parameter sondes to highlight several features of coupled DOC-streamflow dynamics at different timescales. E.g., Saraceno et al. (2009) analyzed a 4-week period including a short-duration storm event. Vaughan et al. (2017) and Fovet et al. (2018) focused on hysteresis in C-Q curves across many storms in catchments with different land use. Mistick and Johnson (2020) analyzed seasonal- and storm-scale DOC responses in clear-cut and forested headwater streams. Blaurock et al. (2021) highlighted the dependency on topography and antecedent wetness conditions. Koenig et al. (2017), Werner et al. (2019), Shogren et al. (2021), and Fazekas et al. (2020) performed multi-year investigations of the C-Q behaviour across multiple sites and timescales.

This paper contributes to the ongoing effort to improve understanding of the related dynamics of streamflow and DOC concentration spatial variability across different timescales. Our investigation focused on a Mediterranean headwater catchment (Turbolo River, southern Italy) characterized by dry and hot summer climate enhancing network intermittency. The catchment was equipped with two multi-parameter sondes at two outlets, an upstream section closing a quasi-pristine sub-catchment and a downstream section closing a catchment affected moderately by human activities (agriculture and villages). More than two-year (May 2019 to November 2021) continuous high-frequency measurements of several chemical-physical parameters were recorded, including DOC-related parameters like fDOM, streamwater temperature and turbidity. On-site measurements were complemented by several samples collected during January-April 2021, aimed at characterizing the catchment and calibrating the fDOM-DOC transfer function. Furthermore, hydrometeorological observations, including discharge at the analyzed sections, were continuously performed.

The study addresses the interrelated dynamics of DOC concentration, river discharge, and other hydrometeorological variables across multiple timescales in a Mediterranean headwater catchment. This general purpose was fulfilled through two specific objectives, which were addressed by exploiting a novel, simple procedure for the correction of recorded fDOM values that does not rely on extensive laboratory measurements: i) the assessment of the seasonal variability of DOC background values related to several hydrometeorological parameters in two nested sections characterized by different land uses; ii) the evaluation of the DOC concentration-discharge relationships at the storm event timescale, considering season- and site-dependence, aimed at uncovering the main mobilization and transport mechanisms. For both the timescales

considered in this study (storm event and seasonal), the difference in DOC response of the two nested cross-sections was analyzed to infer the dependence of DOC dynamics on scale properties and other landscape features.

2 Data and Methods

2.1 Study area

The study area is the upper Turbolo creek catchment (Figure 1), closed at the Fitterizzi gauge (183 m a.s.l.), in southern Italy, a drought-prone area (Mendicino and Versace, 2007), for which an increasing drying scenario is projected (Senatore et al., 2022a). The catchment area is approximately 7 km^2, with an elevation of up to 1005 m a.s.l. The Turbolo creek originates from the Calabrian Coastal Range, which is dominated by strongly altered and fractured crystalline-metamorphic rocks that entail widespread slope instability and have overall high permeability. The geology allows ample groundwater recharge and storage that sustains almost perennial flow at the Fitterizzi gauge. Steep slopes characterize the catchment on the metamorphic rocks in the west. In the eastern part, slopes are less steep but affected by water erosion processes, inducing shallow landslides and soil creep (Senatore et al., 2020).

The channel network consists of two main forks: the southern one (red-contoured on the map) is the San Nicola creek, 2 km^2 wide, in whose closing section (231 m a.s.l.) a gauging station was installed. San Nicola is a quasi-pristine sub-catchment on which only an abandoned settlement is located. The average elevation of the catchment closed at the San Nicola gauge is 600 m a.s.l. The northern fork reflects some more relevant anthropogenic effects, with more agricultural areas (mainly non-irrigated arable land and olive groves) and the village of Mongrassano with an adjoining sewage treatment plant sized for about 500 equivalent inhabitants. The average elevation of the catchment (closed at the Fitterizzi gauge) is 491 m a.s.l.

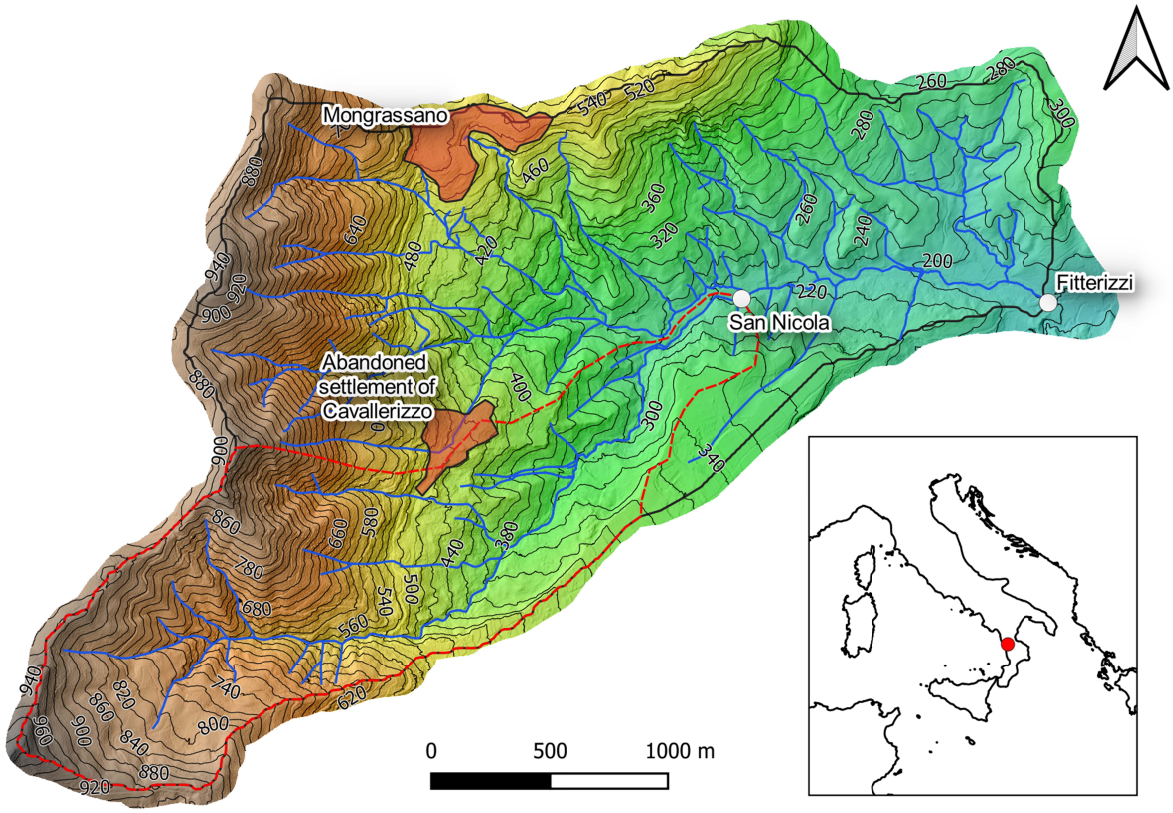

Figure 1. The Turbolo catchment closed at the Fitterizzi outlet. The sub-catchment closed at the San Nicola gauge is contoured by a dashed red line.

2.2 Continuous-time monitoring and manual sampling of water quality

Several chemical-physical parameters were recorded continuously with an hourly time step starting from May 2019 by two multiparametric probes located in the San Nicola (SN) and Fitterizzi (FIT) sites. Monitoring is ongoing, but the results presented here relate to observations performed until 25 November 2021. Two YSI EXO2™ multi-parameter water quality sondes with 7 sensor ports, including a central wiper port, were used. Among the many parameters monitored (namely, ammonia NH3, specific conductance SpCond, Fluorescent Dissolved Organic Matter fDOM, nitrate ions NO3 -N, dissolved oxygen DO, ammonium ions NH4 + -N, redox potential ORP, salinity Sal, total dissolved solids TDS, pH, temperature T and turbidity), Table 1 shows the availability in time for both SN and FIT of fDOM, T and turbidity, needed for DOC calculation.

Continuous observations were supported by discrete monitoring carried out in January-April 2021, when 59 samples were collected on-field and analyzed in the laboratory according to Italian (APAT-IRSA) standards to achieve reference DOC values, used for the correction of measured fDOM values. Besides DOC measurements, several other physico-chemical parameters were measured to characterize the catchment in a larger picture and validate further continuous observations.

Finally, meteo-hydrological observations carried out at both sites were available for the whole period. Specifically, a weather station and a water stage gauge were installed in FIT,

managed by the Regional Agency for the Protection of the Environment (ARPACal), while a water stage gauge operated in SN until March 2021.

Table 1. Data sampling timesheet.

FIT			SN		
Start date	End date	Hourly samples	Start date	End date	Hourly samples
22/05/2019 18:00	19/11/2019 11:00	4338	22/08/2019 18:00	16/12/2019 12:00	2779
16/01/2021 13:00	06/10/2021 06:00	6306	05/01/2020 11:00	30/01/2020 10:00	600
18/10/2021 14:00	26/11/2021 00:00	923	05/04/2020 10:00	25/11/2020 10:00	5617
			01/12/2020 11:00	25/03/2021 10:00	2736
	Total	11567		Total	11732

2.3 Correction of measured fDOM values

In the aim of acquiring DOC timeseries starting from fDOM measurements, the first correction was applied to the raw data to account for the fDOM signal decrease as a function of temperature implied by the increase of non-radiative deactivation pathways (Watras et al., 2011):

$$fDOM_T = fDOM/[1 + \rho(T_m - T_r)] \quad (1)$$

In the above equation, T_m and T_r are measured and reference temperatures in °C, and ρ is a specific temperature attenuation coefficient ($°C^{-1}$) equal to -0.01$°C^{-1}$ (Exo User Manual, 2020).

Then, a suspended particle attenuation factor *k* was estimated to correct the values of $fDOM_T$ using the following equation (Downing et al., 2012):

$$fDOM_{corr} = \frac{fDOM_T}{e^{k*turb}} \quad (2)$$

where *turb* is the turbidity.

The factor $k = 0.004 \pm 0.001$ FNU^{-1} was calibrated using water samples collected under various conditions and analyzed in the laboratory (Figure 2).

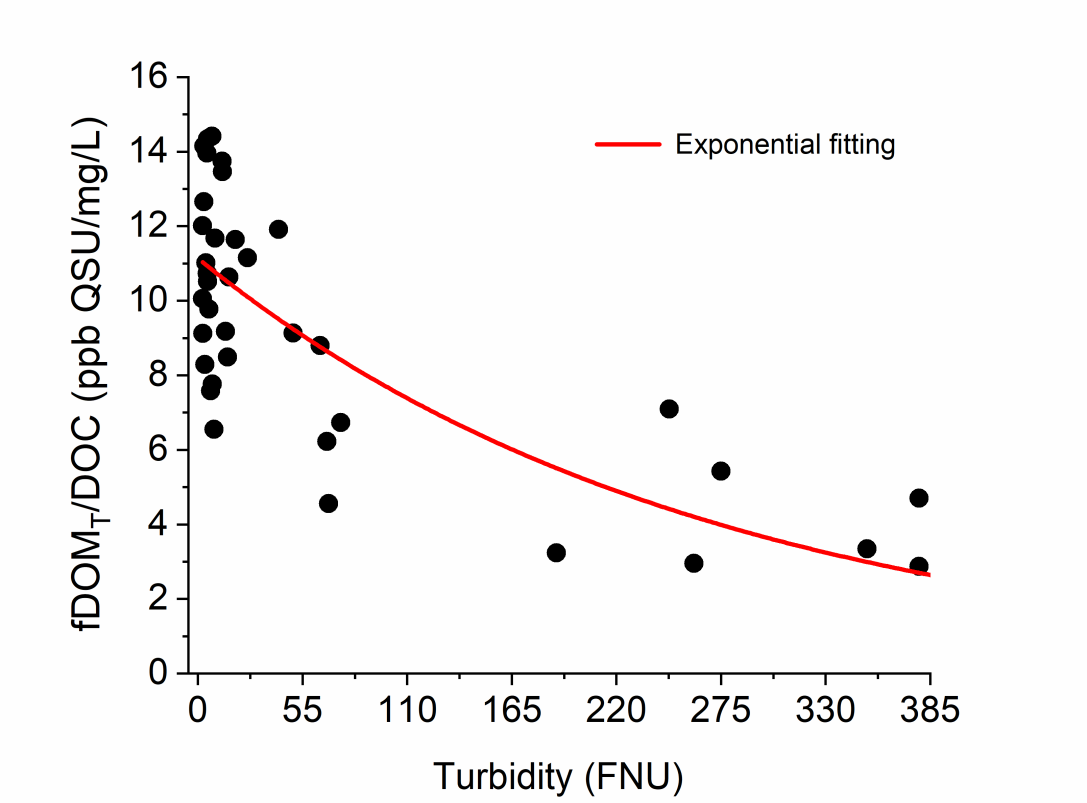

Figure 2. Dispersion plot of the parameter fDOM$_T$/DOC as a function of the turbidity.

Finally, assuming a linear relationship between $fDOM_{corr}$ and DOC:

$$DOC = m \cdot fDOM_{corr} + c \quad (3)$$

The concentration of DOC was estimated. The parameters at eq. (3) were calibrated through linear fitting (using c = 0.8 ± 0.2 and m = 0.054 ± 0.007, Figure 3).

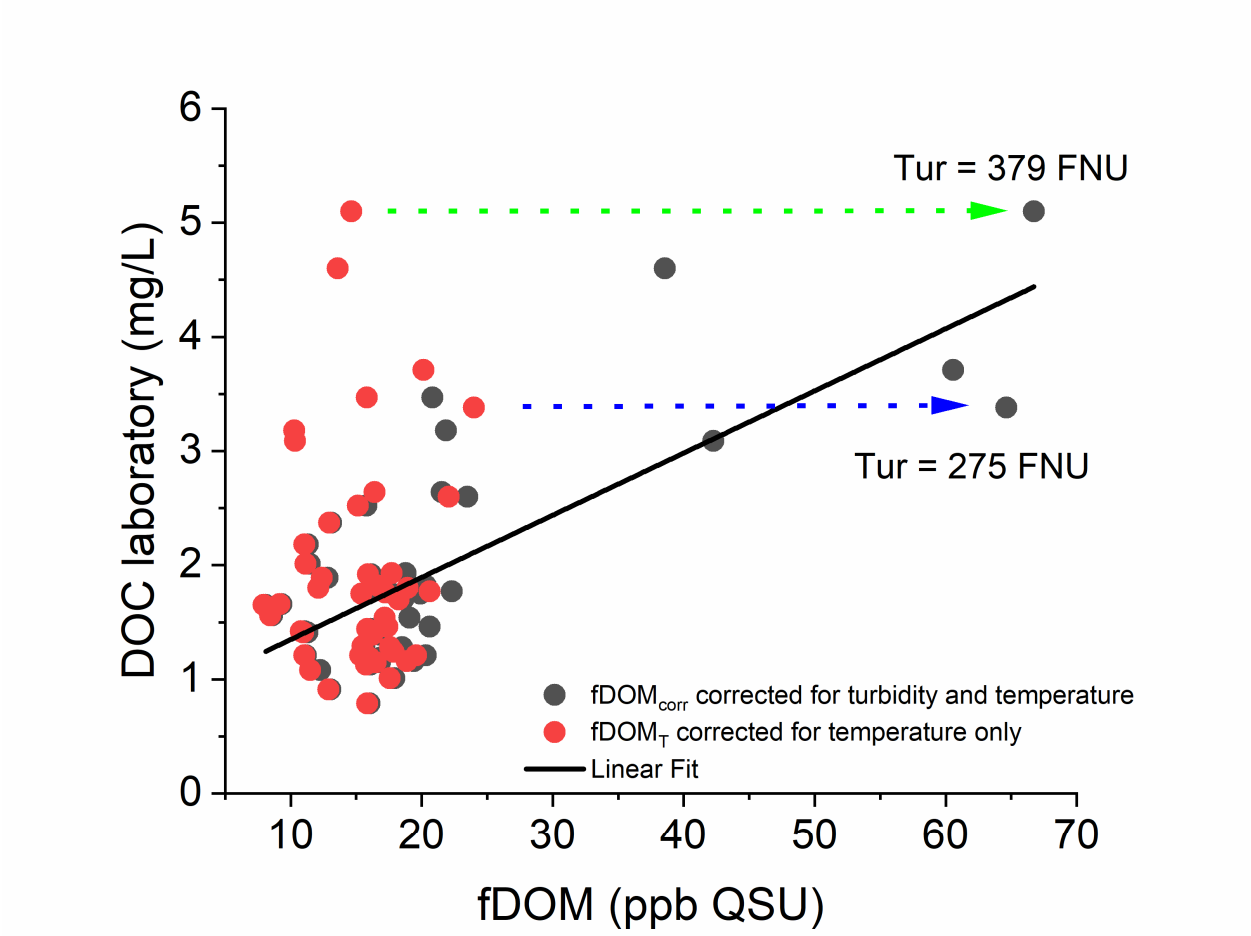

Figure 3. Correlation analysis between the laboratory DOC values measured on discrete samples and the corresponding $fDOM_{corr}$ values (grey circles). The corresponding $fDOM_T$ values are also reported (red circles).

For turbidity values much higher than those used to estimate the factor *k*, equation (2) could not be applied. Therefore, for continuous measurements with turbidity values higher than 600 FNU, DOC values were extrapolated using multiple linear regressions of discharge and accumulated precipitation from 1 up to 12 previous hours. Such regressions reached R^2 values up to 0.7 compared to observations.

2.4 Event Selection and Indices Calculation

A set of 29 focus events for each sub-catchment were identified during the study period following the approach proposed by Landson et al. (2013). At first, the baseflow was separated from quickflow using the following basic filter equations:

$$q_f(i) = \begin{cases} \alpha q_f(i-1) + \frac{(1-\alpha)}{2}[q(i) - q(i-1)] & for\ q_f(i) > 0 \\ 0 & otherwise \end{cases} \quad (4)$$

$$q_b(i) = q(i) - q_f(i) \quad (5)$$

Where $q_f(i)$, $q(i)$, and $q_b(i)$ are the quickflow, the streamflow, and the baseflow response at the ith sampling time (hourly), and α the filter parameter. This iterative method must be run multiple times (called *passes*) forward and backward. Thereafter, the Baseflow Index (BFI), defined as the ratio between the baseflow and the streamflow volume, was used to identify the events. The events selection based on this method was performed through the "hydroEvents" package in Software R using $\alpha = 0.925$, while the appropriate number of passes to separate the baseflow for hourly data was chosen equal to 9, as suggested by Landson et al. (2013). The method adopted not always detected events in both catchments during the same storm. Furthermore, some minor events, though automatically detected, were discarded due to the very low flow associated, especially in the small San Nicola creek.

The hysteresis index HI and the flushing index FI were calculated to evaluate the dynamics of DOC concentration in the analyzed basin, which is mobilized and transported by storm events.

The hysteresis index HI indicates a clockwise or counterclockwise behaviour in the concentration-discharge (C-Q) relationship (Lloyd et al., 2016, Vaughan et al., 2017). For each event, the HI index was calculated starting from the normalized values of discharges and DOC concentrations:

$$Q_{i,norm} = \frac{Q_i - Q_{min}}{Q_{max} - Q_{min}} \quad (6)$$

$$C_{i,norm} = \frac{C_i - C_{min}}{C_{max} - C_{min}} \quad (7)$$

where Q_i and C_i are the discharge and the DOC concentration at the ith time step, Q_{min} and Q_{max} are the maximum and minimum discharge values, respectively, and C_{min} and C_{max} are the maximum and minimum DOC concentrations of the storm event. These normalized concentrations $C_{i,norm}$ were interpolated by linear regression using two adjacent measurements with an interval of 2%. For the same intervals (called j), the hysteresis index HI_j was calculated as follows:

$$HI_j = C_{j,rising} - C_{j,falling} \quad (8)$$

where $C_{j,rising}$ and $C_{j,falling}$ are the DOC concentrations in the rising and falling limb, respectively. The final hysteresis HI (ranging from -1 to +1) of each storm event was obtained by averaging all HI_j values. Positive HI values indicate a clockwise hysteresis, while negative values indicate a counterclockwise hysteresis.

The flushing index (FI) evaluates the increase of concentration, i.e., flushing effect (positive values), or the decrease of concentration, i.e., diluting (negative values) effect of DOC concentration on the rising limb (Butturini et al. 2008, Vaughan et al. 2017). The FI index is defined as:

$$FI = C_{Qpeak,norm} - C_{initial,norm} \quad (9)$$

where $C_{Qpeak,norm}$ and $C_{initial,norm}$ are the normalized DOC concentrations at the peak of discharge and the beginning of the storm, respectively.

3 Results

3.1 Seasonal variability of background DOC concentration

The mean concentration of dissolved organic carbon across the monitoring campaign (2019-2021) for FIT and SN were 1.7 ± 0.3 mg l^{-1} and 2.1 ± 0.5 mg l^{-1}, respectively. These are relatively low values in agreement with typical DOC concentrations in freshwater (≤ 5 mg l^{-1}) (Stumm and Morgan, 1996). Concentrations between the two sites might not be directly comparable because the two recording periods do not entirely overlap. However, reducing the statistics only to the 91 non-rainy days with overlapping observations, DOC concentrations were higher in the SN section (1.8 ± 0.3 mg l^{-1} and 1.9 ± 0.4 mg l^{-1} for FIT and SN, respectively). Slightly higher background values for the upstream monitoring section can be due to the enhanced biomass production and decomposition and the steeper topography of the upstream forested catchment.

Table 2 reports the descriptive statistics on the background values (days in the absence of rain) of FIT and SN sites for the entire monitoring campaign. Box and whisker plots of the DOC showing seasonal trends are given in Figure 4 for both locations. The analysis was conducted on average daily values, and the set of data corresponding to each site was also divided into four categories corresponding to calendar seasons - spring (Sp), summer (S), autumn (A) and winter (W). The two sites showed partially contrasting behaviour. For FIT, the downstream site, the highest average DOC was recorded in autumn, with a descending order of A> S> W> Sp. In SN, the upstream site, the descending order was similar. Still, the highest average DOC was observed in summer (S> A> W> Sp) instead of autumn, probably due to the greater availability of organic material in the surrounding pristine area that during the summer is converted into DOC by photochemical processes. Furthermore, lower autumn temperatures in SN than in FIT due to the higher mean altitude of the contributing catchment inhibit DOC production and export. The analysis suggested that the difference between mean and median values is larger in winter for both sites. This result is connected to the more frequent high-discharge events observed in winter, whose effects can be seen on the non-rainy days considered in this analysis. The one-way ANOVA statistical analysis showed that the four data sets associated with each season were significantly different (FIT $p > 2.97 \times 10^{-43}$; SN $p > 1.70 \times 10^{-71}$).

328 **Table 2.** Descriptive statistics on the data set of seasonal background DOC values (Sp: spring; S:
329 summer; A: autumn; W: winter).

330

	DOC Fitterizzi (mg l^{-1})				DOC San Nicola (mg l^{-1})			
	Sp	S	A	W	Sp	S	A	W
Min	0.93	1.38	1.73	1.23	1.37	2.03	1.13	1.37
Max	2.27	2.76	2.43	3.78	2.09	3.61	2.74	2.8
Mean	1.36	1.78	1.94	1.61	1.58	2.61	2.08	1.64
SD	0.22	0.19	0.17	0.47	0.17	0.34	0.26	0.36
Median	1.28	1.79	1.89	1.45	1.54	2.57	2.13	1.50
N° obs	92	162	58	33	64	102	78	47

331

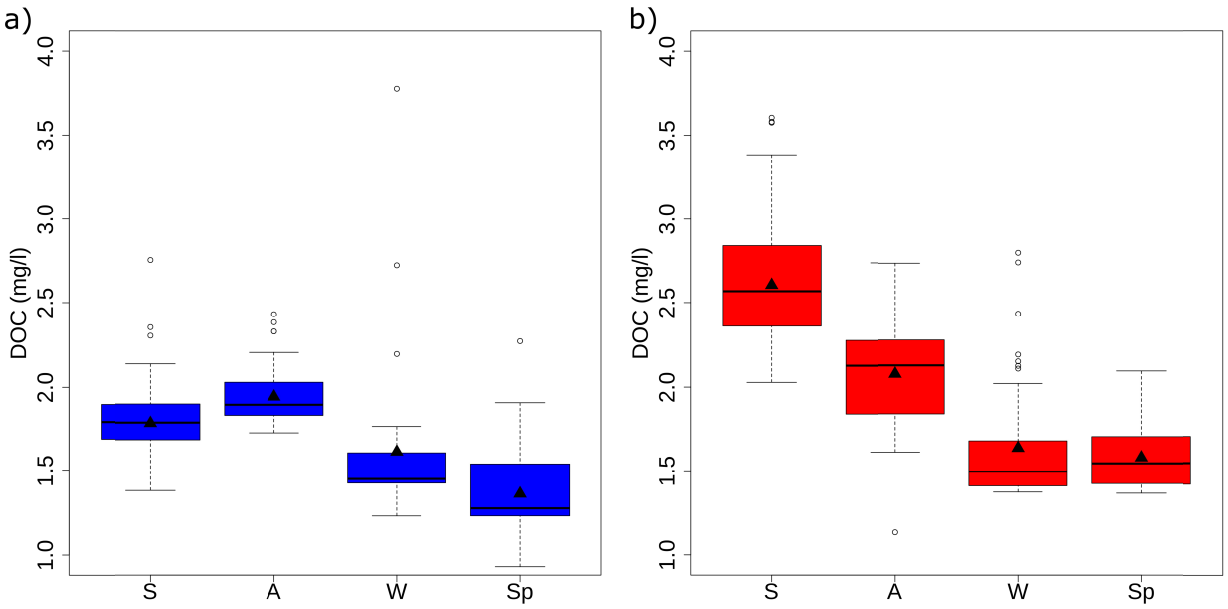

332

333 **Figure 4.** Box and whisker plots of temporal variation of background seasonal DOC values at
334 Fitterizzi and San Nicola stations. Black triangles represent seasonal means.

335

336 To find potential correlations between DOC and key hydrometeorological parameters
337 recorded in FIT, the data were further processed by multivariate data statistical analysis. Figure 5
338 shows the principal component analysis, including DOC and water temperature, air temperature,
339 solar radiation, and discharge. For both sites, PC1 and PC2 altogether explained more than 80%
340 of the total variance, and seasonal clusters could be distinguished with a clear temporal
341 trajectory. Both PCA plots confirm the univariate statistical analysis presented before, indicating
342 higher DOC concentrations were found mainly in summer and, in addition, provide us with
343 further interesting insights because the DOC was negatively affected by the discharge. Indeed,
344 the DOC decreased in a counterclockwise direction from summer to spring. The other
345 meteorological parameters examined positively correlate to DOC since they determined the
346 weather conditions in summer and spring. The DOC was higher in summer due to the
347 concentration effect that the catchment undergoes during this season. However, solar radiation

and temperature may strongly affect the quantity and quality of the DOC through the enhancement of several photocatalytic degradation processes of dissolved organic matter (Stumm and Morgan, 1996).

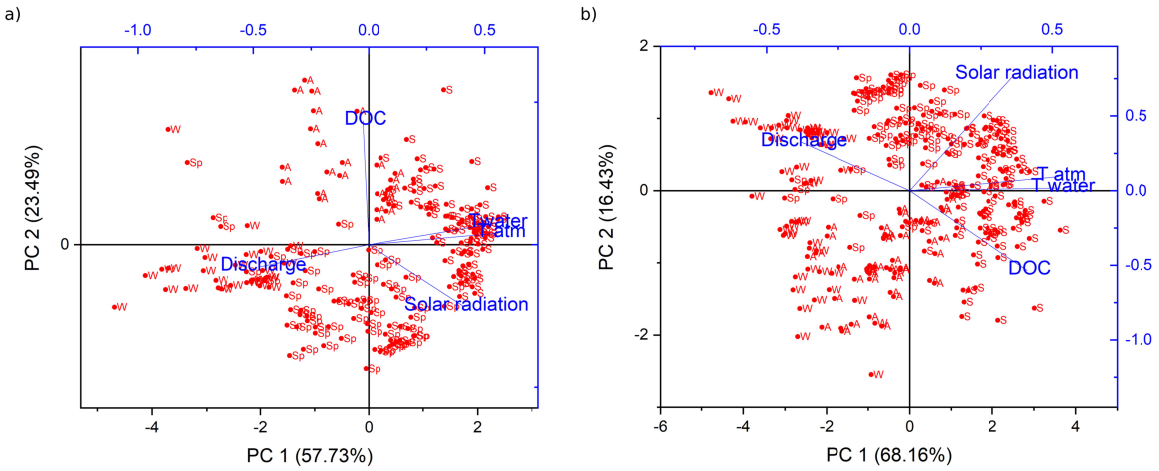

Figure 5. Principal component analysis for background seasonal data sets collected in a) Fitterizzi and b) San Nicola.

3.2 Hydrological controls on DOC export

Most of the export through streamflow occurred relatively quickly, i.e. during high flow events. Discharges above Q10 (i.e., the flow equalled or exceeded only 10% of the time) were responsible for 79% of the total yield in FIT (which is equal to $15.3 \cdot 10^3$ kg in 11567 hours) and 69% in SN ($4.4 \cdot 10^3$ kg in 11732 hours). Figure 6 shows the steep slopes of the flow duration curves in both sites, emphasising the high flow variability and the significant impact of quickflow. Corresponding normalized accumulated DOC load curves are also quite convex. The lower convexity of the SN DOC load curve highlights the relatively more consistent DOC contribution in this more forested catchment with moderate to high discharges.

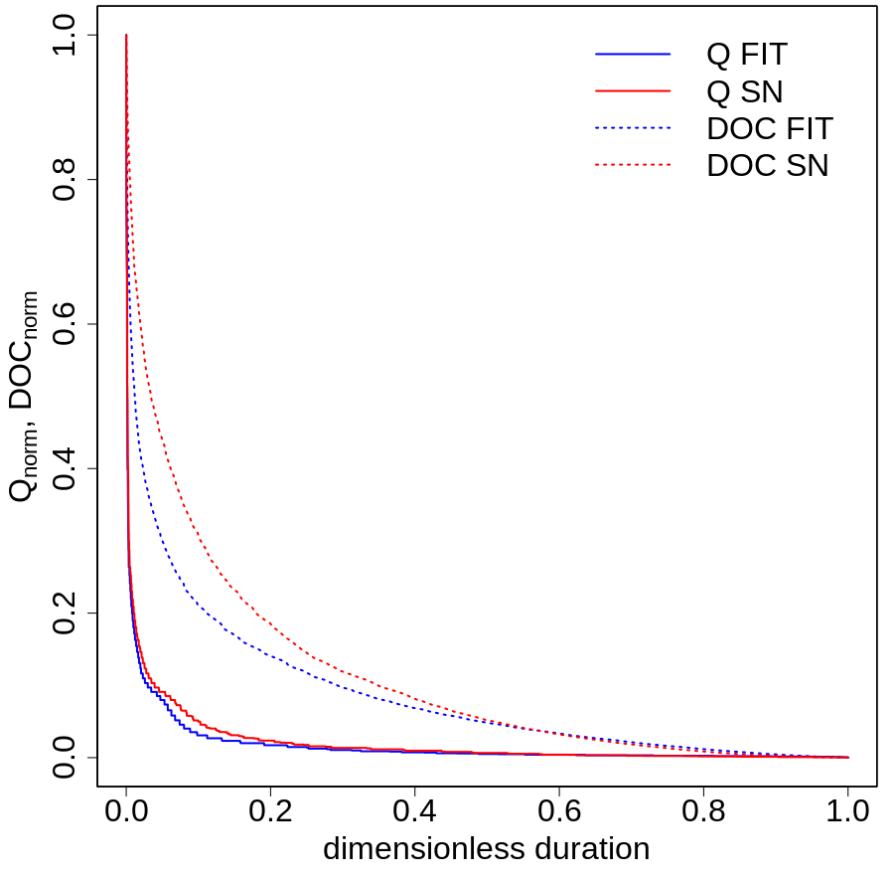

Figure 6. Flow duration curves and corresponding normalized accumulated DOC loads for SN and FIT. It is noteworthy that, while flow duration curves are increasing by definition, corresponding load curves are not because DOC load could be higher with lower discharge values. Nevertheless, this behaviour, which can be detected especially in the low flow tail, is of little significance in this case.

The behaviour of DOC concentrations in FIT and SN were evaluated by comparing 3760 data (hourly time step) acquired simultaneously at both sections during August-November 2019 and January-March 2021. Figure 7 shows that DOC concentration was generally higher in FIT (61% of the time) than in SN. This result, which overturns the indications obtained in the previous seasonal analysis, highlights the importance of the rain/discharge events determining the highest concentration values. The total yield measured in the overlapping measurements period was equal to $12.5 \cdot 10^3$ kg and $2.3 \cdot 10^3$ kg, respectively, for FIT and SN, leading to a ratio between the two total yields of 5.4, which is higher than the ratio between the two catchment areas, approximately equal to 3.5.

The FIT catchment is characterized, overall, by a flatter topography. It is influenced by the significant contribution of the upstream northern fork, having different (less forested, more agricultural) land use and more relevant water erosion processes. It is plausible that DOC sources' connection to the active drainage network in FIT is more dependent on rain events. On the other hand, the SN discharge regime, mainly controlled by groundwater sources with lower

DOC concentration (mountain springs), can reduce the effect of DOC sources' contribution activated by rain events. Indeed, for the overlapping period, DOC concentrations were more positively correlated to the discharge observed in FIT than SN (correlation coefficient *r* equal to 0.65 and 0.34, respectively). This result is consistent with the behaviour of the accumulated DOC load curves in Figure 6, confirming the more substantial impact of high flows in FIT on DOC yield.

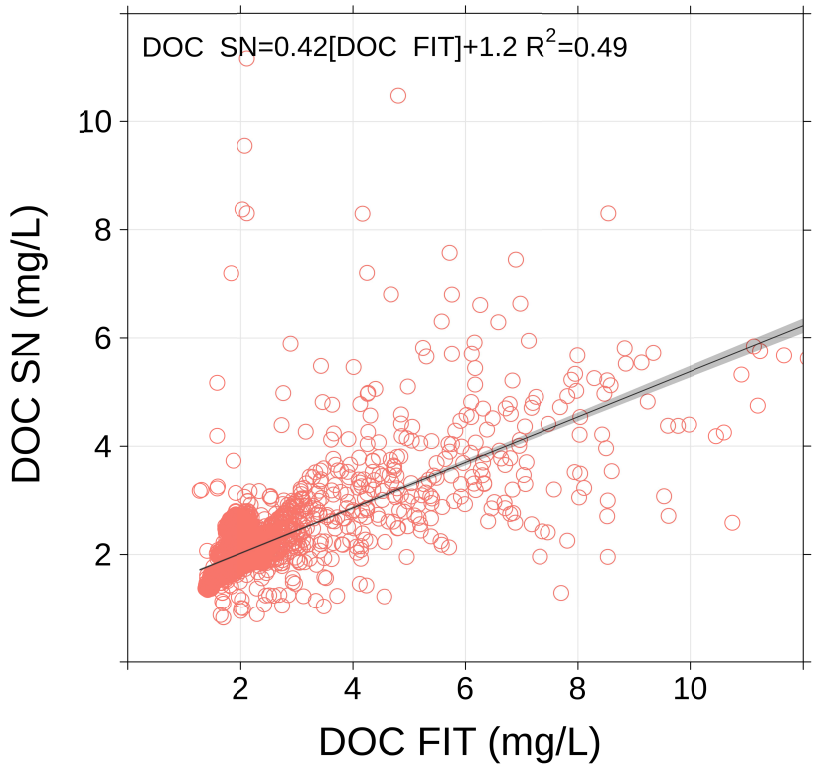

Figure 7. Comparison between simultaneous FIT and SN DOC observations.

The importance of storms and consequent high flows in the regulation of DOC export stands at the basis of the event-based analysis shown in the following. 29 events were selected for each station, 19 representing the response produced in the two sections by the same storm.

Tables 3 and 4 provide some statistics on the selected events. Mean and maximum discharge values were higher in FIT (average values of 0.627 m^3s^{-1} and 1.517 m^3s^{-1}, respectively) than in SN (average values of 0.208 m^3s^{-1} and 0.487 m^3s^{-1}, respectively). Consistently with results shown in Figure 7, mean and maximum DOC concentrations were higher in FIT (average values of 4.03 mg l^{-1} and 8.45 mg l^{-1}, respectively) than in SN (average values of 3.31 mg l^{-1} and 6.78 mg l^{-1}, respectively).

404 **Table 3.** Storms statistics for FIT. Dates marked with * are also considered in SN.

Start date/time	End date/time	Time (h)	Mean discharge ($m^3 s^{-1}$)	Max discharge ($m^3 s^{-1}$)	Mean DOC ($mg l^{-1}$)	Max DOC ($mg l^{-1}$)	HI	FI
28/05/2019 06:00	29/05/2019 00:00	18	0.103	0.179	2.38	5.61	-0.27	0.17
15/07/2019 20:00	16/07/2019 15:00	19	0.097	0.309	7.05	19.88	-0.26	0.28
23/09/2019 22:00	24/09/2019 15:00	17	0.027	0.057	3.14	6.17	-0.51	0.10
07/10/2019 02:00*	08/10/2019 07:00	29	0.065	0.217	4.43	8.83	0.17	1.00
03/11/2019 21:00*	04/11/2019 17:00	20	0.080	0.217	5.03	9.78	0.03	0.73
05/11/2019 14:00*	07/11/2019 17:00	51	0.049	0.260	2.60	5.76	-0.05	0.38
11/11/2019 16:00	12/11/2019 16:00	24	0.083	0.146	4.16	7.32	0.04	0.65
13/11/2019 00:00*	14/11/2019 03:00	27	0.121	0.362	4.35	8.53	0.00	0.90
17/01/2021 13:00*	18/01/2021 17:00	28	0.370	1.226	3.50	8.54	0.27	0.99
23/01/2021 04:00*	23/01/2021 19:00	15	0.508	1.956	4.42	10.75	0.10	0.41
23/01/2021 18:00*	24/01/2021 05:00	11	0.506	1.165	4.14	10.75	0.31	0.00
24/01/2021 03:00*	25/01/2021 14:00	35	2.182	6.796	7.38	17.72	-0.03	0.52
25/01/2021 17:00*	26/01/2021 13:00	20	2.471	5.200	6.40	12.08	-0.02	0.59
31/01/2021 14:00*	01/02/2021 14:00	24	1.224	2.407	4.31	7.57	-0.09	0.04
31/01/2021 22:00*	01/02/2021 14:00	16	1.404	2.407	4.92	7.57	0.00	0.36
01/02/2021 21:00*	02/02/2021 12:00	15	1.536	2.812	4.53	8.02	0.11	0.04
08/02/2021 00:00*	09/02/2021 00:00	24	0.684	1.564	2.48	6.15	0.26	0.57
09/02/2021 00:00*	10/02/2021 00:00	24	0.734	1.290	3.01	5.06	-0.02	0.79
10/02/2021 13:00*	11/02/2021 13:00	24	1.644	4.721	5.31	12.99	0.20	0.54
13/02/2021 09:00*	14/02/2021 02:00	17	1.352	2.707	3.91	6.33	0.27	0.92
14/03/2021 16:00*	15/03/2021 15:00	23	0.225	0.542	2.47	6.11	-0.11	0.88
19/03/2021 19:00*	20/03/2021 19:00	24	0.598	1.564	3.84	7.05	0.33	0.84
20/03/2021 16:00*	22/03/2021 05:00	37	1.071	2.219	4.49	9.13	0.18	0.17
23/04/2021 12:00	24/04/2021 23:00	35	0.524	1.226	3.22	5.85	0.23	0.68
17/07/2021 13:00	19/07/2021 17:00	52	0.034	0.396	2.31	6.14	-0.36	0.70
26/08/2021 15:00	27/08/2021 02:00	11	0.028	0.060	3.30	6.87	-0.15	0.32
11/09/2021 06:00	11/09/2021 22:00	16	0.060	0.182	2.81	3.35	-0.38	0.78
25/10/2021 14:00	26/10/2021 09:00	19	0.088	0.158	2.65	4.28	-0.14	0.87
01/11/2021 17:00	02/11/2021 15:00	22	0.308	1.638	4.46	10.73	0.07	0.77

405

406 **Table 4.** Storms statistics for SN. Dates marked with * are also considered in FIT.

Start date/time	End date/time	Time (h)	Mean discharge ($m^3 s^{-1}$)	Max discharge ($m^3 s^{-1}$)	Mean DOC (mg l^{-1})	Max DOC (mg l^{-1})	HI	FI
07/10/2019 12:00*	08/10/2019 02:00	14	0.019	0.044	3.23	7.58	0.01	0.33
03/11/2019 14:00*	04/11/2019 18:00	28	0.013	0.069	3.40	8.36	0.06	0.20
05/11/2019 14:00*	07/11/2019 17:00	51	0.009	0.056	2.18	5.49	-0.30	0.23
12/11/2019 22:00*	14/11/2019 01:00	27	0.027	0.077	2.81	7.31	-0.21	0.20
09/12/2019 08:00	10/12/2019 13:00	29	0.112	0.311	1.57	2.14	-0.01	0.52
04/07/2020 12:00	05/07/2020 09:00	21	0.018	0.050	2.91	5.40	-0.11	0.59
08/08/2020 08:00	09/08/2020 07:00	23	0.010	0.025	3.30	4.58	0.17	0.78
25/09/2020 15:00	26/09/2020 20:00	29	0.028	0.140	3.87	7.00	0.04	0.96
28/09/2020 08:00	29/09/2020 07:00	23	0.084	0.480	4.26	11.26	-0.01	0.69
15/10/2020 06:00	16/10/2020 04:00	22	0.035	0.077	3.02	5.36	0.38	0.73
08/12/2020 21:00	10/12/2020 01:00	28	0.399	0.959	2.65	4.36	-0.17	-0.34
30/12/2020 21:00	31/12/2020 10:00	13	0.339	0.517	5.32	10.99	-0.06	-0.18
09/01/2021 13:00	10/01/2021 13:00	24	0.136	0.430	4.54	9.52	-0.19	0.10
15/01/2021 06:00	16/01/2021 09:00	27	0.156	0.304	4.07	7.61	-0.16	0.17
17/01/2021 13:00*	18/01/2021 17:00	28	0.102	0.337	3.41	8.30	-0.16	0.12
23/01/2021 04:00*	23/01/2021 19:00	15	0.158	0.537	3.46	6.80	-0.09	0.35
23/01/2021 18:00*	24/01/2021 05:00	11	0.136	0.320	3.48	7.20	-0.04	-0.20
24/01/2021 02:00*	25/01/2021 08:00	30	0.641	1.867	4.56	9.13	-0.20	-0.41
25/01/2021 17:00*	26/01/2021 13:00	20	0.680	1.428	3.38	5.62	-0.24	0.19
31/01/2021 14:00*	01/02/2021 14:00	24	0.338	0.661	2.90	4.78	-0.14	-0.11
31/01/2021 22:00*	01/02/2021 14:00	16	0.390	0.661	3.08	4.78	-0.06	0.02
01/02/2021 21:00*	02/02/2021 12:00	15	0.421	0.773	3.22	4.57	-0.03	0.09
08/02/2021 00:00*	09/02/2021 00:00	24	0.190	0.430	2.21	5.89	-0.09	1.00
09/02/2021 00:00*	10/02/2021 00:00	24	0.203	0.354	2.49	6.24	-0.17	0.15
10/02/2021 13:00*	11/02/2021 12:00	23	0.463	1.297	3.27	5.26	-0.04	0.64
13/02/2021 09:00*	14/02/2021 02:00	17	0.371	0.744	3.41	10.48	0.22	0.16
14/03/2021 16:00*	15/03/2021 15:00	23	0.062	0.149	2.33	5.71	-0.21	0.84
19/03/2021 18:00*	20/03/2021 17:00	23	0.166	0.430	3.31	6.61	0.12	0.43
20/03/2021 16:00*	21/03/2021 21:00	29	0.328	0.610	4.27	8.42	0.27	0.70

407

408 Analyzing the indices accounting for DOC concentration during storms helps understand
409 the nature of the relevant mobilization and export processes driving DOC dynamics in stream
410 water. Figure 8 provides a comprehensive overview of the catchment response during these
411 events by comparing the two sites' hysteresis (HI) and flushing (FI) indices. In FIT and SN,
412 positive FI values largely prevailed (only SN showed 5 out of 29 slightly negative values). A
413 positive flushing index means that the DOC sources in the regions that contribute to the fast
414 response of the catchment (root zone and riparian areas) are abundant enough to increase
415 concentration when discharge increases (rising limb of the hydrograph).

416 HI results provided more contrasting information. In FIT, HI values were equally
417 subdivided into positive and negative, with few values practically equal to zero. In SN, 8 values
418 out of 29 were positive, but the general behaviour was not very different from FIT. HI values for
419 the two sections during the 19 simultaneous events were correlated quite well ($r = 0.63$).
420 Negative HI values represent counterclockwise behaviour in the concentration–discharge (C-Q)

graphs, meaning that DOC concentration is higher in the falling limb of the hydrograph than in the rising. This behaviour generally occurs when the primary DOC sources are relatively far and hydraulically disconnected from the active river network at the beginning of the storm or when DOC transport is lower than water flux into the channel. Negative values of HI might also imply that the export process is transport-limited, i.e., the process ceases because of the reduced transport capacity when the water drains towards the watercourse. On the other hand, positive HI values mean clockwise behaviour in the C-Q graphs, higher concentrations in the rising limb, the proximity of the major DOC sources to the active network, and source-limited process, i.e., despite a still sustained water flow from the catchment to the river network, DOC concentration reduces in time. Therefore, the HI index allows quantifying event hysteresis dynamics, even with complex patterns (Williams, 1989) that are not easily interpretable. Overall, the slightly higher number of negative HI values in SN can be correlated to lower hydraulic connectivity of the upstream mountainous, steep catchment, presenting more accentuated flow spatial intermittency than FIT, as is typical for the headwater catchments.

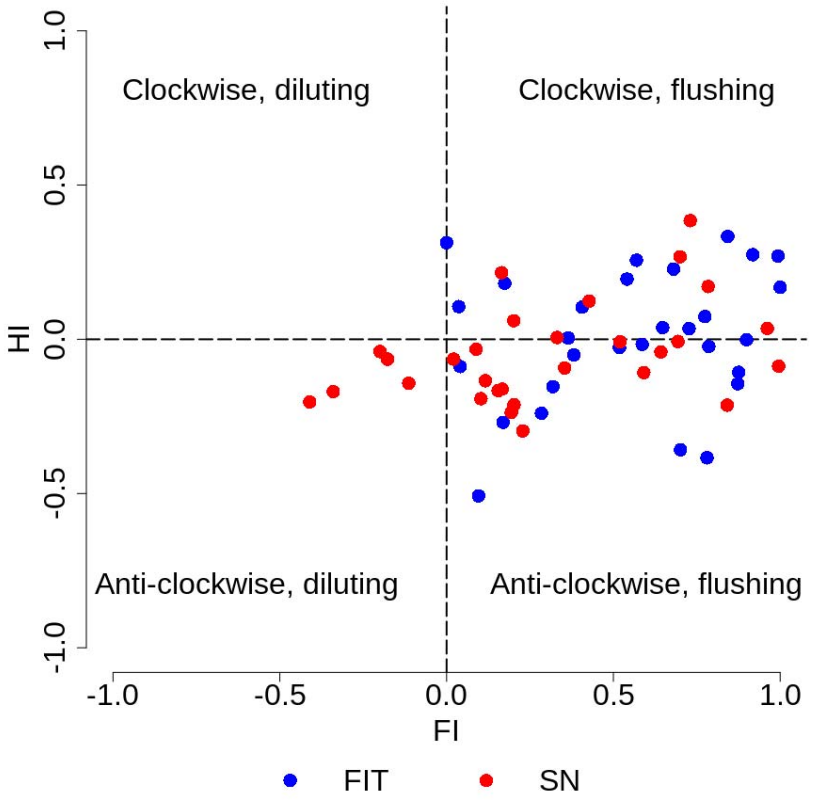

Figure 8. Storm hysteresis index (HI) versus storm flushing index (FI) for FIT and SN.

Beyond the observed differences between the upstream and downstream sections, no general rules exhaustively explained the occurrence of clockwise/counterclockwise hysteresis during flow events. In SN, positive HI values were observed at the end of the winter, consistently with enhanced hillslope-channel hydraulic connectivity at the end of the wet season. Three positive HI events were detected from 13.02.2021 to 21.03.2021 (Table 4), also providing the

highest loads due to the corresponding high discharges. Nevertheless, four events with HI > 0 occurred in early autumn (07.10.2019, 03.11.2019, 25.09.2020 and 15.10.2020) and one even in summer (08.08.2020). However, all these events were characterized by very low flows (the maximum peak flow overcame 0.1 m^3s^{-1} only in one case), therefore providing a relatively low contribution in terms of DOC load. The maximum discharges of the events were weakly negatively correlated to HI values (r = -0.21), while correlations with FI were stronger (r = -0.43). The latter result can be explained by considering that DOC removal might become supply-limited during high-intensity events. Indeed, the average maximum discharge of the 5 diluting events in SN was almost double (0.865 m^3s^{-1}) that of all events.

The positive HI values in FIT events occurred only in autumn and winter (Table 3). The only exception was given by one positive HI event in spring (23.04.2021), which, however, took place immediately after the wet winter season. Furthermore, the most negative index values occurred all in late spring/summer, with generally dry conditions. HI values were positively correlated with the maximum discharges of the events (r = +0.32), while FI correlations were weaker than SN (r = -0.12).

Figure 9 shows examples of hydrographs, DOC chemographs and the corresponding C-Q relations for FIT and SN in the case of positive and negative HI values. Specifically, the 17.01.2021 event (Figs. 9a-d) concerned both catchments, with opposite HI signs (-0.16 and +0.27, in SN and FIT, respectively). This event is peculiar because the DOC concentration evolution had similar behaviour and was synchronous in the two sections, occurring at the same time as the FIT discharge peak, while the discharge peak in SN was brought forward by one hour. In SN, despite the flow reduction, DOC concentration increased for the hour following the peak flow, contrasting the decrease in the total load. This result can be interpreted considering that the time needed to reach the peak flow in FIT corresponded to the time required to mobilize the primary DOC sources in both catchments, while the peak flow in SN was attained earlier. Rainfall peak intensity in the Fitterizzi rain gauge (only 4.4 mm hr^{-1}) occurred in the same hour as the rainfall peak in SN. However, this rain gauge is not within the SN catchment; hence some rainfall features in this catchment, like the exact amount and timing, could have been missed.

Figs. 9e-f show a summer event (15.07.2019) for FIT, with a negative HI value (-0.26) and significantly high DOC concentration. This event was characterized by a higher rainfall amount than the previous case (32.6 mm hr^{-1} two hours before the peak flow, 8.6 mm hr^{-1} one hour before and 15.8 mm hr^{-1} at the peak flow time). The suddenly increased hydraulic connection in the river network given by this typical summer rain shower following a dry period contributed to higher DOC concentration values in the falling limb.

Finally, an event in SN with a positive HI value (+0.27) is shown (Figs. 9g-h). This event occurred at the end of the winter (wet) period (20.03.2021), concatenating two consecutive smaller events with clockwise evolution (Figure 9h). Interestingly, discharge was lower and DOC concentration higher in the first event, consistently with the assumption that, for positive HI values, the export processes are source-limited. In this case, rainfall intensity was low (maximum 3.8 mm hr^{-1} at the Fitterizzi gauge station).

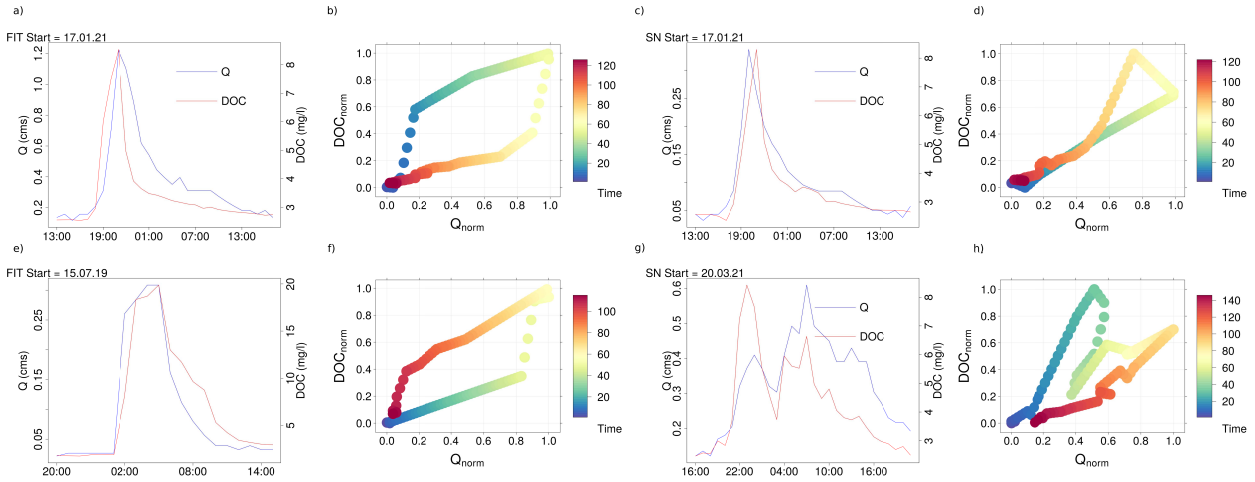

Figure 9. DOC concentrations and hydrographs and corresponding DOC–Q hysteresis during the events.

The higher correlation of HI with discharges in FIT and the more pronounced seasonality suggests that its variability can be partially explained by focusing on the antecedent weather conditions, influencing soil moisture and hydraulic connectivity. On the other hand, it can be tested if similar mechanisms were activated even at SN despite the lower correlation with discharge. Figure 10 shows the HI correlation with the precipitation accumulated over different time intervals, ranging from two hours to ten days before the discharge peak value. For both SN and FIT, a relative correlation peak was found for approximately 0.5 days of rainfall accumulation. After that, SN correlation decreased, while HI variability in FIT was more clearly explained by precipitation accumulated in the previous 6 to 7 days, up to $r = 0.38$ ($p < 0.001$). The lower correlation of SN with more extended accumulation periods can be explained by its smaller extent (hence, faster response to storm events) and the relatively higher contribution of groundwater to its discharge. On the other hand, network connectivity in FIT looks more sensitive to the precipitation accumulated over a longer time interval. However, r values were low overall.

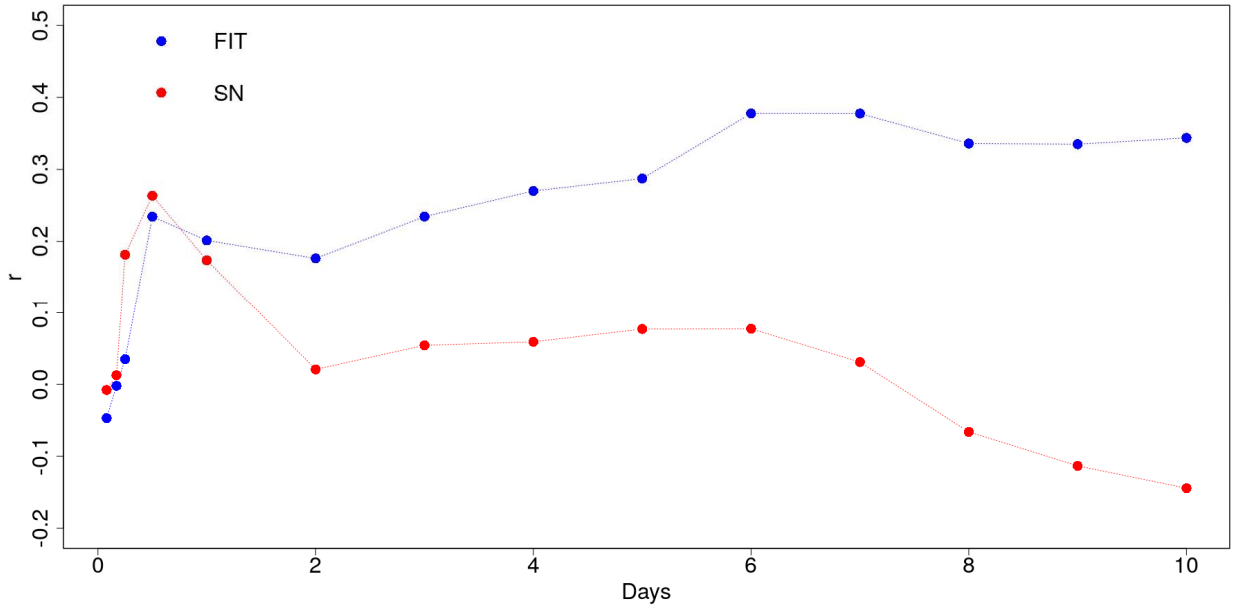

Figure 10. HI correlation with precipitation accumulated in different time intervals (FIT and SN).

The scatter plots of HI versus accumulated precipitation for the most highly correlated time intervals (i.e., 6 days for FIT and 0.5 days for SN; Fig. 11) highlight the non-linear nature of the correlation. Scattered points were interpolated through generalized additive models (GAMs, Hastie and Tibshirani, 1986; 1990), which are smooth, nonparametric functions. Especially in FIT (Figure 11a), GAMs highlighted the non-linear relation between HI and antecedent precipitation. In general, for low accumulated precipitation values, DOC export was transport-limited (HI < 0). Then, for higher accumulation values, meaning continuous (not necessarily intense) precipitation in the considered interval, DOC sources tended to be flushed, and the process became source-limited (HI > 0). Nevertheless, when accumulated precipitation was high enough, it could mobilize other DOC sources, and the process tended to return transport-limited. The event with the highest antecedent 6-day rainfall in FIT started on 25.01.2021 after several other events had just happened. Indeed, the C-Q graph of this event (not shown) includes more than one loop and is characterized as complex, according to Rose et al. (2018). The relation between antecedent precipitation and hysteresis described for FIT is much more roughly sketched out in the smaller SN catchment (Figure 11b), for which a smaller accumulation interval was also considered.

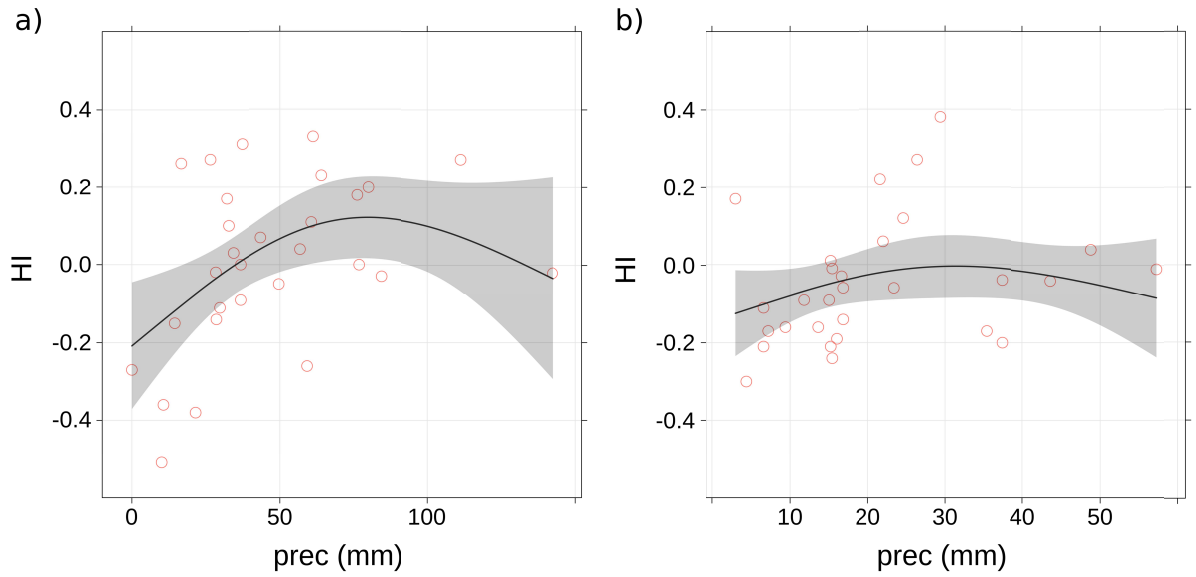

519

520 **Figure 11.** HI vs accumulated precipitation: a) FIT (6-day precipitation); b) SN (0.5-day
521 precipitation).

522

523 **4 Discussion**

524 The seasonal pattern observed for DOC concentration in both sites (Figures 4 and 5)
525 agrees with other studies that reported freshwaters DOC concentration peaking in autumn. In
526 most cases, this seasonality is dependent on discharge (negative correlation), leading to
527 clockwise hysteretic loops with respect to seasons due to lower DOC concentration in
528 winter/spring and higher concentration in summer/autumn periods (Mulholland and Hill, 1997;
529 Aubert et al., 2013; Dawson et al., 2008; Fovet et al., 2018). Figures 12a and 12c show the
530 seasonal hysteretic cycles in the Q-C plane for Fitterizzi and San Nicola. Data refer to the years
531 2021 and 2020, respectively, for which an almost complete series of data across the entire year
532 were available. They confirm the expected pattern for the two sites under investigation, even
533 though an anticipated DOC peak occurred in San Nicola, where the max DOC concentration was
534 observed in late summer/early autumn.

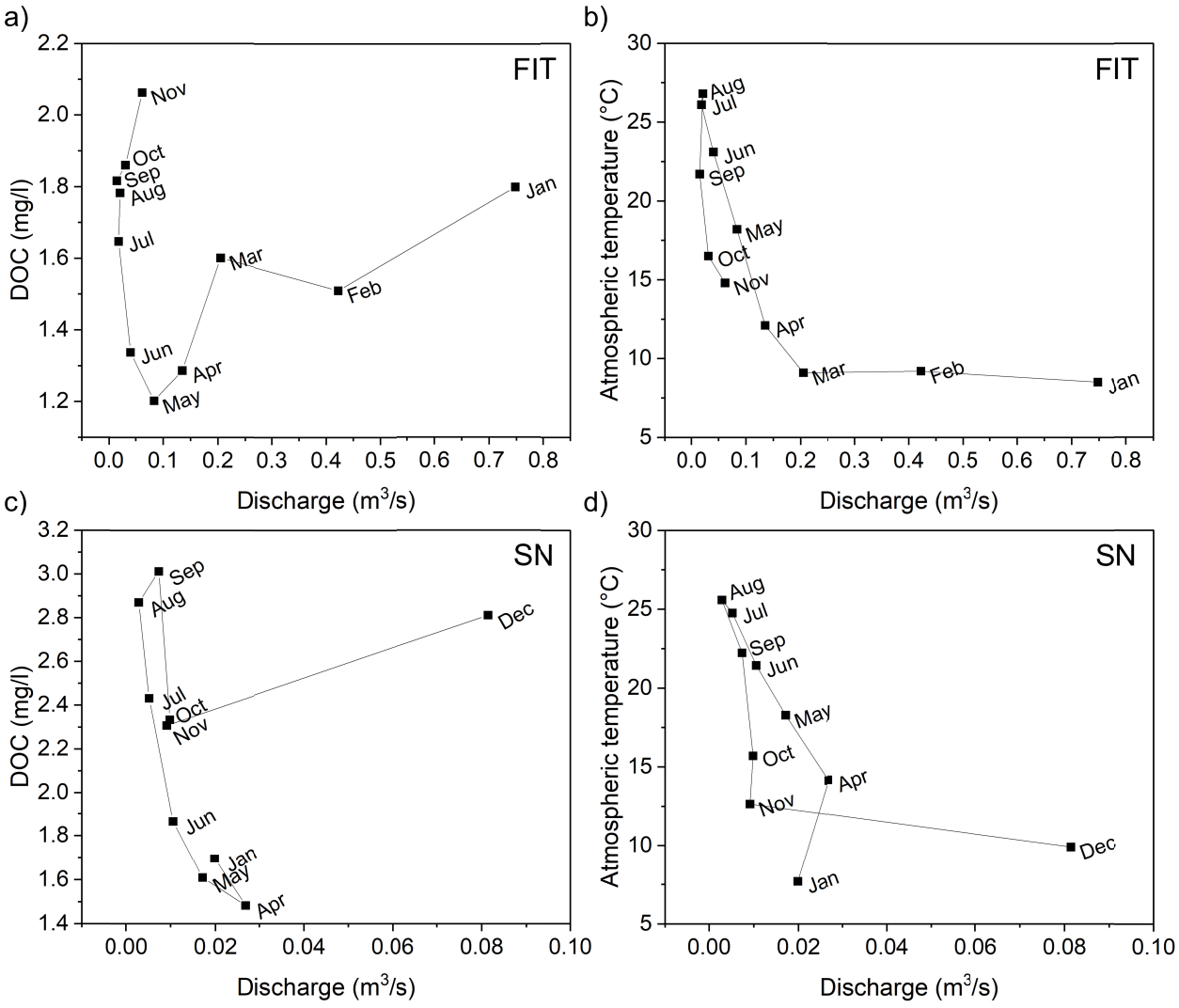

Figure 12. Mean monthly concentrations of a), c) DOC and b), d) mean monthly atmospheric temperature plotted against mean monthly specific discharge for a), b) Fitterizzi (2021), and c), d) San Nicola (2020).

Intra-annual hysteretic loops in the Q-C plane reflect seasonality in the catchment streamflow dynamics and in-stream variation in the rate of net nutrient release and uptake. Therefore, they may show a site-dependent behaviour (Mulholland and Hill, 1997; Brooks et al., 1999; Dawson et al., 2001; Dawson et al., 2008; Aubert et al., 2013), as partially confirmed by our dataset. Differences may be explained through the unlike contribution of the dominant hydrologic pathway and in-stream processes in the two sites. Figures 12b and 12d show the corresponding hysteretic loops for the monthly mean atmospheric temperature, highlighting counterclockwise patterns to discharge for both locations. The peak temperature lagged about one month behind DOC in SN, while there was a larger inertia in the broader and lower elevation FIT catchment. Temperature is a critical hydro-climatic parameter affecting the seasonal pattern of stream water chemistry. Thus, it can be eventually used as an alternative to discharge to understand the intra-annual variability of water quality (Aubert et al., 2013). DOC and

552 temperature were positively correlated in both sites. Though, this correlation was more
553 significant in the San Nicola site, an instance which may explain the differences in the earlier
554 monthly DOC concentration peak observed in San Nicola.

555 The baseflow carries a relatively low amount of DOC, primarily mobilized by individual
556 storms. In agreement with previous studies, DOC peaks were observed during flood events
557 (Vaughan et al., 2017, Rose et al., 2018, Blaurock et al., 2021), when significant DOC
558 enhancement could be measured. As an example, Fovet et al. (2018) recorded an increase
559 $\Delta C = 5 \pm 4\ mg\ C\ l^{-1}$ compared to a concentration of DOC < 1 mg C l^{-1} during baseflow,
560 Blaurock et al. (2021) observed peaks of 10.2-18.6 mg l^{-1} and 8.5-16.9 mg l^{-1} for two sites in
561 comparison to a concentration of 2-3 mg l^{-1} during the baseflow.

562 This case study confirms the influence of the topography on the mechanism of DOC
563 mobilization and export during storms. Similarly to the catchment located in southeastern
564 Germany and analyzed by Blaurock et al. (2021), the DOC was monitored in two different sub-
565 catchments situated in an upper position with steep slopes and in a lower and flatter site. While
566 during the background periods, the DOC concentration was higher in the upstream sub-
567 catchment (i.e., SN), greater concentrations were recorded in the downstream site during the
568 storm events. The DOC average values in response to storm events confirm the results found by
569 Blaurock et al. (2021). They found average values for the 4 events reported equal 3.88 mg l^{-1} and
570 1.75 mg l^{-1} in the lower and upper sub-catchment, respectively. They correlated this behaviour to
571 topography, highlighting that saturated soils are needed in flatter areas to allow efficient lateral
572 water transport through DOC-rich soil layers towards the active river network. Moreover, like in
573 Blaurock et al. (2021), DOC mobilization was generally delayed in the flat lower catchment, as
574 confirmed by the slighter decrease after the peak and hysteretic loops wider than the upper
575 catchment (larger absolute values of HI in 13 cases out of the 19 simultaneous events).

576 In literature test areas, there is a prevalence of counterclockwise loops (negative values
577 of HI) for DOC hysteresis (e.g., 51 counterclockwise compared to only 3 clearly clockwise and
578 46 complex events in Rose et al., 2018; 6 cases out of 8 counterclockwise in Blaurock et al.,
579 2021). Instead, the flushing index FI is mainly positive (Vaughan et al., 2017). In this study, the
580 negative HI values were 21 over 29 and 13 over 29 for SN and FIT, respectively, while negative
581 FI values were only 5 out of 29 for SN and were undetected in FIT. The clockwise loop is likely
582 linked to the total catchment wetness seasonal pattern. Indeed, during or immediately after the
583 end of the wet season, when the catchment water storage is high, the hillslope-channel
584 hydrological connections are favoured compared to other periods, as shown by previous studies
585 in the catchment (Senatore et al., 2021; Micieli et al., 2022). Therefore the DOC peak anticipates
586 the discharge peak describing a clockwise hysteresis. This seasonal dependence of hysteresis is
587 also in line with the results of Fovet et al. (2018). They showed clockwise hysteresis for 62% of
588 events at a high flow period typical of the wet season in a Brittany, Western France catchment.

589 Finally, the study of the correlation between catchment wetness conditions and hysteresis
590 direction was already addressed. Blaurock et al. (2021) found a positive correlation with the
591 rainfall accumulated 14 days before the event started. Our analysis based on a variable
592 accumulation time window confirmed such influence and highlighted different process timings
593 depending on the catchment's size and other features. In larger, flatter catchments, complete
594 hydraulic activation generally requires extended periods. Nevertheless, also precipitation
595 intensity and amount count. We demonstrated that by expanding the analysis to high

precipitation amounts, a non-linear correlation arises, given by the connection of new DOC sources far from the stream.

5 Conclusions

This study presented the results of a long-term monitoring campaign to unveil space and time DOC dynamics in a Mediterranean headwater catchment, relating them to meteorological and hydrological drivers. The different DOC dynamics observed in two nested sites were linked to spatially heterogeneous catchment properties (extent, orographic features, land uses). Two multi-parameter sondes were used to achieve that aim, and high-resolution continuous timeseries of several biogeochemical parameters were obtained.

The analysis relied on an original correction method, requiring water temperature and turbidity measurements to convert the observed fDOM into DOC values. Then, analyses performed at seasonal and storm event timescales provided several insights into DOC mobilization and export processes:

- At the seasonal scale, univariate and multivariate statistical analysis confirmed the climate (seasonal) control on DOC production, with background concentrations increasing in hot and dry summer months due to the combined effect of enhanced photocatalytic degradation and reduced discharge in the channels;
- Comparison of DOC concentrations taken simultaneously over 91 non-rainy days led to slightly higher values in the forested upstream catchment, having steeper topography and, of course, smaller streamflow;
- However, observations made clear the importance of the hydrological regulation of DOC export, significantly activated by high-flow events, with discharge above Q10 being associated with 69% of the total yield in the upstream and 79% in the downstream site;
- Also, the increased hillslope-channel connectivity all over the downstream catchment triggered by hydrological processes overturned the results of the seasonal background analysis, with DOC concentration higher in the downstream site considering the 3760 simultaneous observations at the hourly time scale;
- DOC sources proved to be plentiful in the zones contributing to the catchment's fast response in both sites, being able to increase concentration during almost all the storm events. Instead, the limiting factor of DOC export processes varied by season and location. In the steep upstream catchment with accentuated spatial intermittency, generally, such processes were transport-limited, while in the downstream catchment, more source-limited processes were observed;
- Therefore, the hysteresis index was more positively correlated to antecedent precipitation in the downstream catchment. However, such correlation was not linear since new DOC sources were activated with exceptionally high accumulated rainfall values, and the process tended to be transport-limited again.

Overall, the study demonstrated the importance of high-resolution measurements to explain DOC dynamics at multiple time scales with a quantitative approach. However, though supported by laboratory measurements, the on-site recording showed some inherent weaknesses, primarily when high discharge was associated with high turbidity values, requiring the statistical

retrieval of DOC peak values. Such a drawback can be partially overcome with increased on-site discrete automatic sampling during storm events and subsequent laboratory analysis. One of the further developments of the research goes towards this direction. Furthermore, it will be necessary to focus more on the processes' scaling properties, taking advantage of both the measurements in this and other sites, to support modelling approaches and contribute to a better understanding of the global carbon cycle.

Acknowledgements, Samples, and Data

We thank the "Centro Funzionale Multirischi" of the Calabrian Regional Agency for the Protection of the Environment for providing the observed meteorological dataset.

This study was supported by the European Research Council (ERC) DyNET project funded through the European Community's Horizon 2020 - Excellent Science - Programme (grant agreement H2020-EU.1.1.-770999).

Weather data are delivered, upon request, by the "Centro Funzionale Multirischi – ARPACAL" (http://www.cfd.calabria.it/). The experimental data collected for this study are available at Senatore et al. (2022b).

References

Ahmadi, B., Ahmadalipour, A., & Moradkhani, H. (2019). Hydrological drought persistence and recovery over the CONUS: a multi-stage framework considering water quantity and quality. *Water Research*, 150, 97–110. https://doi.org/10.1016/j.watres.2018.11.052

Aitkenhead-Peterson, J. A., Smart, R. P., Aitkenhead, M. J., Cresser, M. S., & McDowell, W. H. (2007). Spatial and temporal variation of dissolved organic carbon export from gauged and ungauged watersheds of Dee Valley, Scotland: Effect of land cover and C V N, *Water Resource Research,* 43, W05442. https://doi.org/10.1029/2006WR004999

Aubert, A. H., Gascuel-Odoux, C., & Merot, P. (2013). Annual hysteresis of water quality: A method to analyse the effect of intra and inter-annual climatic conditions. *Journal of Hydrology*, 478, 29–39. http://dx.doi.org/10.1016/j.jhydrol.2012.11.027

Basu, N.B., Destouni, G., Jawitz, J.W., Thompson, S.E., Loukinova, N.V., Darracq, A., Zanardo S., et al. (2010). Nutrient loads exported from managed catchments reveal emergent biogeochemical stationarity. *Geophysical Research Letters,* 37 (23), L23404. https://doi.org/10.1029/2010GL045168

Bengtson, P., & Bengtsson, G. (2007). Rapid turnover of DOC in temperate forests accounts for increased CO2 production at elevated temperatures. *Ecology Letters,* 10 (9), 783–790. https://doi.org/10.1111/j.1461-0248.2007.01072.x

Bertuzzo, E., Helton, A.M., Hall, R.O., & Battin, T.J. (2017). Scaling of dissolved organic carbon removal in river networks. *Advances in Water Resources*, 110, 136-146. https://doi.org/10.1016/j.advwatres.2017.10.009

Blaurock, K., Beudert, B., Gilfedder, B. S., Fleckenstein, J. H., Peiffer, S., & Hopp, L. (2021). Low hydrological connectivity after summer drought inhibits DOC export in a forested

676 headwater catchment. *Hydrology and Earth System Sciences,* 25(9), 5133-5151.
677 https://doi.org/10.5194/hess-25-5133-2021

678 Botter, G., Vingiani, F., Senatore A., Jensen C., Weiler M., McGuire K., et al. (2021).
679 Hierarchical climate-driven dynamics of the active channel length in temporary streams.
680 *Scientific Reports,* 11, 21503. https://doi:10.1038/s41598-021-00922-2

681 Brooks P. D., McKnight D. M., & Bencala K. E. (1999). The relationship between soil
682 heterotrophic activity, soil dissolved organic carbon (DOC) leachate, and catchment-scale
683 DOC export in headwater catchments. *Water Resource Research,* 35:1895–1902.
684 https://doi:10.1029/1998WR900125

685 Butman, D., & Raymond, P. A. (2011). Significant efflux of carbon dioxide from streams and
686 rivers in the United States. *Nature Geoscience*, 4(12), 839– 842.
687 https://doi.org/10.1038/ngeo1294

688 Butturini, A., Alvarez, M., Bernal, S., Vazquez, E., & Sabater F. (2008), Diversity and temporal
689 sequences of forms of DOC and NO3-discharge responses in an intermittent stream:
690 Predictable or random succession?, *Journal of Geophysical Research,* 113, G03016,
691 https://doi.org/10.1029/2008JG000721

692 Chaplot, V. & Mutema, M. (2021). Sources and main controls of dissolved organic and inorganic
693 carbon in river basins: A worldwide meta-analysis. *Journal of Hydrology*, 603, 126941.
694 https://doi.org/10.1016/j.jhydrol.2021.126941

695 Chen, S., Zhong, J., Li, C., Liu, J., Wang, W., Xu, S., & Li, S. L. (2021), Coupled effects of
696 hydrology and temperature on temporal dynamics of dissolved carbon in the Min River,
697 Tibetan Plateau. *Journal of Hydrology*, 593, 125641.
698 https://doi.org/10.1016/j.jhydrol.2020.125641

699 Chorover, J., Derry, L.A., & McDowell, W.H., (2017). Concentration-discharge relations in the
700 critical zone: Implications for resolving critical zone structure, function, and evolution.
701 *Water Resources Research*, 53(11), 8654-8659. https://doi.org/10.1002/2017WR021111

702 Cole, J.J., Prairie, Y.T., Caraco, N.F., McDowell, W.H., Tranvik, L.J., Striegl, R.G., et al., AU
703 (2007). Plumbing the global carbon cycle: Integrating inland waters into the terrestrial
704 carbon budget. *Ecosystems*, 10, 171-184. https://doi.org/10.1007/s10021-006-9013-8

705 Dawson J.J.C., Billett M.F., & Hope D. (2001). Diurnal variations in the carbon chemistry of two
706 acidic upland streams in northeast Scotland. *Freshwater Biology,* 46, 1309–1322.
707 https://doi:10.1046/j.1365-2427.2001.00751.x.

708 Dawson J.J.C., Soulsby, C., Tetzlaff, D., Hrachowitz, M., Dunn S. M., & Malcolm, I. A., (2008).
709 Influence of hydrology and seasonality on DOC exports from three contrasting upland
710 catchments. *Biogeochemistry,* 90, 93–113. https://doi.org/10.1007/s10533-008-9234-3.

711 Downing B.D., Pellerin, B.A., Bergamaschi, B.A., Saraceno, J.F., & Kraus T.E.C. (2012).
712 Seeing the light: The effects of particles, dissolved materials, and temperature on in situ
713 measurements of DOM fluorescence in rivers and streams. *Limnology and*
714 *Oceanography: Methods,* 10: 767-775. https://doi.org/10.4319/lom.2012.10.767

715 Exo User Manual, Advanced Water Quality Monitoring Platform, YSI, a Xylem brand. Yellow
716 Springs, OH, US, 2020.

Fazekas, H.M., Wymore, A.S., & McDowell, W.H. (2020). Dissolved organic carbon and nitrate concentration-discharge behavior across scales: Land use, excursions, and misclassification. *Water Resources Research,* 56, e2019WR027028. https://doi.org/10.1029/2019WR027028

Fovet, O., Humbert, G., Dupas, R., Gascuel-Odoux, C., Gruau, G., Jaffrézic, A., et al. (2018), Seasonal variability of stream water quality response to storm events captured using high-frequency and multi-parameter data. *Journal of Hydrology*, 559, 282-293. https://doi.org/10.1016/j.jhydrol.2018.02.040

Freeman, C., Evans, C.D., Monteith, D.T., Reynolds, B., & Fenner, N., 2001. Export of organic carbon from peaty soils. *Nature,* 412, 785. https://doi.org/10.1038/35090628

Giesbrecht, I.J. W., Tank, S.E., Frazer, G.W., Hood, E., Gonzalez Arriola, S.G., Butman, D.E., et al. (2022). Watershed classification predicts streamflow regime and organic carbon dynamics in the Northeast Pacific Coastal Temperate Rainforest. *Global Biogeochemical Cycles,* 36, e2021GB007047. https://doi.org/10.1029/2021GB007047

Godsey, S.E., Kirchner, J.W., & Clow D.W. (2009). Concentration–discharge relationships reflect chemostatic characteristics of US catchments. *Hydrological Processes: An International Journal,* 23(13), pp.1844-1864. https://doi.org/10.1002/hyp.7315

Hastie, T., & Tibshirani, R. (1986). Generalized Additive Models, *Statistical Science,* Vol. 1, No 3, 297-318.

Hastie, T., & Tibshirani, R. (1990). Generalized Additive Models, Chapman & Hall/CRC, New York/Boca Raton

Humbert, G., Jaffrezic, A., Fovet, O., Gruau, G., & Durand P. (2015), Dry season length and runoff control annual variability in stream DOC dynamics in a small, shallow groundwater-dominated agricultural watershed, *Water Resource Research,* 51, 7860–7877, https://doi.org/10.1002/2015WR017336

Jones, T.D., Chappell, N.A., & Tych, W. (2014). First dynamic model of dissolved organic carbon derived directly from high-frequency observations through contiguous storms. *Environmental science & technology,* 48(22), pp.13289-13297. https://doi.org/10.1021/es503506m

Koenig, L.E, Shattuck, M.D., Snyder, L.E., Potter, J.D., & McDowell, W.H. Deconstructing the effects of flow on DOC, nitrate, and major ion interactions using a high-frequency aquatic sensor network. *Water Resources Research,* 53, 10,655–10,673. https://doi.org/10.1002/2017WR020739

Ladson, A., Brown, R. Neal B. & Nathan, R. (2013). A standard approach to baseflow separation using the Lyne and Hollick filter. *Australasian Journal of Water Resources,* 17(1), pp.25-34. https://doi.org/10.7158/13241583.2013.11465417

Lloyd, C.E., Freer, J.E., Johnes, P.J., & Collins, A.L. (2016). Testing an improved index for analysing storm discharge–concentration hysteresis. *Hydrology and Earth System Sciences,* 20(2), pp.625-632. https://doi.org/10.5194/hess-20-625-2016

Lowe W.H., Likens G.E., & Power M.E. (2006). Linking scales in stream ecology. *Bioscience,* 56(7):591–597. https://doi.org/10.1641/0006-3568(2006)56[591:LSISE]2.0.CO;2

McGuire, K.J., Torgersen, C.E., Likens, G.E., Buso, D.C., Lowe, W.H., & Bailey, S.W. (2014). Network analysis reveals multiscale controls on streamwater chemistry. *Proceedings of the National Academy of Sciences,* 111 (19) 7030-7035. https://doi.org/10.1073/pnas.1404820111

Mehring, A.S., Lowrance, R.R., Helton, A.M., Pringle, C.M., Thompson, A., Bosch, D.D., & Vellidis, G. (2013). Interannual drought length governs dissolved organic carbon dynamics in blackwater rivers of the western upper Suwannee River basin. *Journal of Geophysical Research: Biogeosciences,* 118, 1636–1645. https://doi.org/10.1002/2013JG002415

Mendicino, G., & Versace, P. (2007). Integrated Drought Watch System: A Case Study in Southern Italy. *Water Resources Management,* 21:8, 21(8), 1409–1428. https://doi.org/10.1007/S11269-006-9091-6

Micieli, M., Botter, G., Mendicino, G., & Senatore, A (2022). UAV Thermal Images for Water Presence Detection in a Mediterranean Headwater Catchment. *Remote Sensing,* 14, 108. https://doi.org/10.3390/rs14010108

Mistick, E., & Johnson, M.S. (2020). High-frequency analysis of dissolved organic carbon storm responses in headwater streams of contrasting forest harvest history. *Journal of Hydrology,* 590, p.125371. https://doi.org/10.1016/j.jhydrol.2020.125371

Monteith, D.T., Stoddard, J.L., Evans, C.D., de Wit, H.A., Forsius, M., Høgåsen, T., Wilander, A., et al., (2007). Dissolved organic carbon trends resulting from changes in atmospheric deposition chemistry. *Nature,* 540, 527–540. https://doi.org/10.1038/nature06316

Morison, M.Q., Higgins, S. N., Webster, K. L., Emilson, E. J. S., Yao, H., & Casson, N. J. (2022), Spring coherence in dissolved organic carbon export dominates total coherence in Boreal Shield forested catchments. *Environmental Research Letters*, 17, 014048. https://doi.org/10.1088/1748-9326/ac462f

Mulholland, P.J., & Hill, W.R., 1997. Seasonal patterns in streamwater nutrient and dissolved organic carbon concentrations: separating catchment flow path and in-stream effects. *Water Resource Research,* 33 (6), 1297–1306. https://doi.org/10.1029/97WR00490

Musolff, A., Schmidt, C., Selle, B., & Fleckenstein, J. H. (2015). Catchment controls on solute export. *Advances in Water Resources*, 86, 133–146. https://doi.org/10.1016/j.advwatres.2015.09.026

Parr T.B., Inamdar S.P., & Miller M.J. (2019). Overlapping anthropogenic effects on hydrologic and seasonal trends in DOC in a surface water dependent water utility. *Water Research*, 148, 407-415. https://doi.org/10.1016/j.watres.2018.10.065

Pellerin, B.A. & Bergamaschi B.A., (2014). Optical sensors for water quality. Lakeline, Spring, *North American Lake Management Society,* pp.13-17

Rose, L.A., Karwan, D.L., & Godseyet, S.E. (2018). Concentration–discharge relationships describe solute and sediment mobilization, reaction, and transport at event and longer timescales. *Hydrological Processes,* 32(18), pp.2829-2844. https://doi.org/10.1002/hyp.13235

798 Roulet, N. & Moore, T.R., (2006). Browning the waters. *Nature*, 444(7117), pp.283-284.
799 https://doi.org/10.1038/444283a

800 Rovelli, L., Attard, K. M., Heppell, C. M., Binley, A., Trimmer, M., & Glud, R. N. (2018).
801 Headwater gas exchange quantified from O 2 mass balances at the reach scale. *Limnology*
802 *and Oceanography: Methods,* 16(10), 696– 709. https://doi.org/10.1002/lom3.10281

803 Saraceno, J. F., Pellerin, B.A., Downing, B.D., Boss, E., Bachand, P.A.M. & Bergamaschi B.A.
804 (2009), High-frequency in situ optical measurements during a storm event: Assessing
805 relationships between dissolved organic matter, sediment concentrations, and hydrologic
806 processes, *Journal of Geophysical Research,* 114, G00F09,
807 https://doi.org/10.1029/2009JG000989

808 Seybold, E., Gold, A. J., Inamdar, S. P., Adair, C., Bowden, W. B., Vaughan, M. C. H., et al.
809 (2019). Influence of land use and hydrologic variability on seasonal dissolved organic
810 carbon and nitrate export: insights from a multiyear regional analysis for the northeastern
811 USA, *Biogeochemistry*, 146, 31–49, https://doi.org/10.1007/s10533-019-00609-x

812 Senatore, A., Micieli, M., Liotti, A., Durighetto, N., Mendicino, & G., Botter G. (2021).
813 Monitoring and Modeling Drainage Network Contraction and Dry Down in
814 Mediterranean Headwater Catchments. *Water Resources Research,* 57(6),
815 e2020WR028741. https://doi.org/10.1029/2020WR028741

816 Senatore, A., Fuoco, D., Maiolo, M., Mendicino, G., Smiatek, G., & Kunstmann, H. (2022a).
817 Evaluating the uncertainty of climate model structure and bias correction on the
818 hydrological impact of projected climate change in a Mediterranean catchment. *Journal*
819 *of Hydrology: Regional Studies,* 42, 101120.
820 https://doi.org/10.1016/J.EJRH.2022.101120

821 Senatore, A., Corrente, G.A., Argento, E.L., Castagna, J., Micieli, M., Mendicino, M., Beneduci,
822 A., & Botter, G. (2022b). Seasonal and storm event-based dynamics of dissolved organic
823 carbon (DOC) concentration in a Mediterranean headwater catchment – DATASET.
824 Retrieved from https://researchdata.cab.unipd.it/id/eprint/801 doi:
825 10.25430/researchdata.cab.unipd.it.00000801

826 Shogren, A.J., Zarnetske, J.P., Abbott, B.W., Iannucci, F., Medvedeff, A., Cairns, S., et al.
827 (2021). Arctic concentration–discharge relationships for dissolved organic carbon and
828 nitrate vary with landscape and season. *Limnology and Oceanography,* 66, pp. S197-
829 S215. https://doi.org/10.1002/lno.11682

830 Snyder L., Potter, J.D., & McDowell W.H. (2018). An Evaluation of Nitrate, fDOM, and
831 Turbidity Sensors in New Hampshire Streams. *Water Resources Research,* 54, 2466-
832 2479. https://doi.org/10.1002/2017WR020678

833 Soares, A.R.A., Lapierre, J.F., Selvam, B.P., Lindström G., & Berggren M. (2019). Controls on
834 Dissolved Organic Carbon Bioreactivity in River Systems. *Scientific Reports*, 9:14897.
835 https://doi.org/10.1038/s41598-019-50552-y.

836 Song, X., Sidana L., Kun S., Yang G., & Xuefa W. (2021). Flux and source of dissolved
837 inorganic carbon in a headwater stream in a subtropical plantation catchment. *Journal of*
838 *Hydrology,* 600, 126511. https://doi.org/10.1016/j.jhydrol.2021.126511

839 Stumm, W. & Morgan, J.J. (1996) Aquatic Chemistry, Chemical Equilibria and Rates in Natural
840 Waters. 3rd Edition, *John Wiley & Sons, Inc.,* New York. ISBN: 978-0-471-51185-4

841 Vaughan, M. C. H., Bowden, W. B., Shanley, J. B., Vermilyea, A., Sleeper, R., Gold, A. J. et al.
842 (2017), High-frequency dissolved organic carbon and nitrate measurements reveal
843 differences in storm hysteresis and loading in relation to land cover and seasonality,
844 *Water Resource Research,* 53, 5345–5363. https://doi.org/10.1002/2017WR020491

845 Viza, A., Muñoza, I., Oliva F., & Menéndez M. (2022), Contrary effects of flow intermittence
846 and land uses on organic matter decomposition in a Mediterranean river basin. *Science of*
847 *The Total Environment,* 812, p.151424. https://doi.org/10.1016/j.scitotenv.2021.151424

848 Watras, C.J., Hanson, P.C., Stacy, T.L., Morrison, K.M., Mather, J., Hu, Y.-H., & Milewski P.
849 (2011). A temperature compensation method for CDOM fluorescence sensors in
850 freshwater. *Limnology and Oceanography: Methods,* 9: 296-301.
851 https://doi.org/10.4319/lom.2011.9.296

852 Weiler, M. & McDonnell, J. J. (2006). Testing nutrient flushing hypotheses at the hillslope scale:
853 A virtual experiment approach, *Journal of Hydrology,* 319, 339–356,
854 https://doi.org/10.1016/j.jhydrol.2005.06.040

855 Werner, B. J., Musolff, A., Lechtenfeld, O. J., de Rooij, G. H., Oosterwoud, M. R., &
856 Fleckenstein, J. H. (2019). High-frequency measurements explain quantity and quality of
857 dissolved organic carbon mobilization in a headwater catchment. *Biogeosciences,* 16(22),
858 pp.4497-4516. https://doi.org/10.5194/bg-16-4497-2019

859 Williams, G. P. (1989). Sediment concentration versus water discharge during single hydrologic
860 events in rivers. *Journal of Hydrology,* 111(1–4), 89–106. https://doi.org/10.1016/0022-
861 1694(89)90254-0

862 Worrall, F. & Burt, T.P. (2007). Trends in DOC concentration in Great Britain. *Journal of*
863 *Hydrology,* 346, 81-92, https://doi.org/10.1016/j.jhydrol.2007.08.021

864 Wu, J., Yao, H., Yuan, X., & Lin, B. (2022). Dissolved organic carbon response to hydrological
865 drought characteristics: Based on long-term measurements of headwater streams. *Water*
866 *Research,* 215, p.118252. https://doi.org/10.1016/j.watres.2022.118252

867 Zhong, J., Li, S.L., Ibarra, D.E., Ding, H., & Liu, C.Q. (2020). Solute Production and Transport
868 Processes in Chinese Monsoonal Rivers: Implications for Global Climate Change. *Global*
869 *Biogeochemical Cycles.* https://doi.org/10.1029/2020gb006541